

Multimodal machine learning with large language embedding model for polymer property prediction

Tianren Zhang^{*,†,‡} and Dai-Bei Yang[‡]

[†]*Department of Materials Science and Engineering, University of Delaware, Newark, Delaware 19716, United States*

[‡]*Department of Chemistry, University of Pennsylvania, Philadelphia, Pennsylvania 19104, United States*

E-mail: tianren@udel.edu

Abstract

Contemporary large language models (LLMs), such as GPT-4 and Llama, have harnessed extensive computational power and diverse text corpora to achieve remarkable proficiency in interpreting and generating domain-specific content, including materials science. To leverage the domain knowledge embedded within these models, we propose a simple yet effective multimodal architecture, PolyLLMem, which integrates text embeddings generated by Llama 3 with molecular structure embeddings derived from Uni-Mol, for polymer properties prediction tasks. In our model, Low-rank adaptation (LoRA) layers were also incorporated during the property prediction tasks to refine the embeddings based on our limited polymer dataset, thereby enhancing their chemical relevance for polymer SMILES representation. This balanced fusion of fine-tuned textual and structural information enables PolyLLMem to accurately predict a variety of polymer properties despite the scarcity of training data. Its performance is comparable

to, and in some cases exceeds, that of graph-based models, as well as transformer-based models that typically require pretraining on millions of polymer samples. These findings demonstrate that LLM, such as Llama, can effectively capture chemical information encoded in polymer PSMILES, and underscore the efficacy of multimodal fusion of LLM embeddings and molecular structure embeddings in overcoming data scarcity and accelerating the discovery of advanced polymeric materials.

Introduction

Polymeric materials with their complex architectures and diverse functionalities serve as good candidates for a wide array of applications ranging from everyday consumer products to advanced lightweight aerospace and biomedical devices.^{1,2} Their unique properties, such as high molecular weight, tunable chemical functionality, and versatile mechanical behavior, enable the design of materials that are tailored to specific performance requirements. Accurate prediction of polymer properties can significantly accelerate the materials discovery process, allowing researchers to rapidly identify and optimize promising candidates while reducing reliance on time-consuming and costly experimental trials.³⁻⁸

The intrinsic complexity of polymer structures, coupled with the limited size of available databases, poses significant challenges for accurate property prediction. To overcome those limitations, researchers in polymer fields adapted a variety of strategies that encompass polymer representation, feature extraction, data augmentation, and application of diverse machine learning (ML) architectures to expedite the development of predictive models in polymer research. For instance, similar to Simplified Molecular-Input Line-Entry System (SMILES)⁹ used for small molecules, polymer SMILES including Polymer Simplified Molecular-Input Line-Entry System (PSMILES) and BigSMILES^{10,11} were proposed as an extension of the traditional SMILES notation to describe macromolecular structures, including repeating units, end groups, and connectivity patterns. Furthermore, various molecular descriptors and structural representations, such as Morgan fingerprints, Morgan fingerprint

with frequency, and molecular graphs,^{12–17} have been derived from polymers and utilized as input features for ML models. Those notations and feature extractions enable the standardized digital representation of polymers, facilitating computational analysis, database storage, and interoperability in polymer informatics applications. Additionally, to overcome the limitations imposed by the small size of polymer databases, Ma et al. developed the PIIM database by training a generative model on approximately 12,000 polymers manually collected from PolyInfo and subsequently generating around one million polymers.¹⁸ Similarly, Kuenneth et al. generated a data set of 100 million hypothetical polymers by enumeratively combining chemical fragments extracted from a list of more than 13,000 synthesized polymers.¹¹

With these advances in feature engineering, data augmentation, and database expansion, both classical ML and deep learning models have been employed to enhance polymer property prediction. Among classical ML models, ensemble tree-based models (Random Forests, Gradient Boosting) have emerged as top performers in polymer properties prediction tasks when provided with rich, chemically informed features.^{3,19} Tao et al. conducted a comprehensive benchmark that evaluated 79 different ML models, including linear, tree-based, kernel, and deep learning approaches, on a large glass transition temperature (T_g) dataset using various polymer feature representations (e.g., Morgan fingerprints, RDKit descriptors, learned embeddings, and molecular graphs).^{20,21} They demonstrated that a Random Forest model (RF) using a Morgan fingerprint with substructure frequency could achieve the highest accuracy in predicting T_g . Similarly, Uddin and Fan built an interpretable ML pipeline for T_g , testing nine algorithms (including decision trees, Support Vector Machine, k Nearest Neighbors, various boosting methods, and RF), and found that RF provided the highest predictive R^2 .¹⁶ In addition to tree-based models, Wu et al. successfully applied Support Vector Regression and Gaussian Process to capture nonlinear structure–property relationships in polymers, emphasizing the importance of selecting robust descriptors for reliable predictions.¹⁴

On the deep learning front, architectures such as Graph Neural Networks (GNNs) have been employed to directly learn from polymer molecular graphs, capturing both local atomic environments and global connectivity patterns.²²⁻²⁵ For example, Graph Convolutional Neural Networks (GCNNs) have been widely used to predict the dielectric constant and energy bandgap of polymers,²⁶ as well as T_g and thermal decomposition temperature (T_d) of block copolymers and homopolymers.^{19,27} Gurnani et al. developed polyGNN, a model that learns directly from monomer structures to simultaneously predict multiple polymer properties.²⁸ Similarly, transformer-based models, including ChemBERTa, TransPolymer, and polyBERT, have been pretrained on millions of PSMILES collections to capture rich contextual embeddings, which were subsequently applied to various downstream tasks.^{11,29-31} TransPolymer integrated polymer-specific tokenization scheme to capture not only repeating units and end groups but also connectivity patterns, leading to high performance across a range of polymer properties prediction.²⁹ In addition, approaches such as polyBERT and PolyNC further enhance prediction performance by combining data augmentation, generative models, and multimodal fusion. PolyBERT utilized a massive dataset of 100 million hypothetical polymers to pretrain a chemical language model that can predict multiple properties simultaneously, while PolyNC fused natural language prompts with PSMILES to achieve robust multitask learning.^{11,15} Moreover, multimodal frameworks like MMPolymer³² integrate 3D structural information with 1D sequence data, providing complementary insights that significantly improve predictions for properties sensitive to polymer conformation. Although these deep learning approaches demonstrated high accuracy in the predictions of polymer properties, they typically required careful architecture design and large volumes of real or virtual polymer data for pretraining before being effectively applied to downstream tasks.

Recent advancements in machine learning, particularly with large language models (LLM) like GPT-4 and Llama, have leveraged vast computational resources and extensive text corpora, including materials science literature, to demonstrate remarkable capabilities in understanding, reasoning, and generating domain-specific content.³³⁻³⁸ One study introduced

GenePT, a model that leveraged LLM-derived embeddings from text descriptions of individual genes and single-cell data, and demonstrated performance comparable to or exceeding that of models pretrained on gene-expression profiles from millions of cells for downstream tasks such as gene-property and cell-type classification.³⁹ Inspired by these results, we postulated that LLMs have already been exposed to substantial polymer-related knowledge and are capable of extracting relevant information from polymer texts for downstream tasks such as property prediction. Therefore, in this study, we leveraged an LLM to generate polymer-specific text embeddings. Moreover, to complement these textual embeddings and further enhance predictive capabilities, we incorporated structural embeddings obtained from Uni-Mol, a deep learning model specifically designed to encode detailed molecular structures.⁴⁰ Uni-Mol has been pretrained on millions of 3D molecular representations of small molecules, enabling it to capture critical structural and chemical features necessary for chemical prediction tasks. By integrating embeddings from both the LLM and Uni-Mol, we developed PolyLLMem, a multimodal neural network tailored specifically for polymer property prediction. This approach substantially reduces the effort required to design and pretrain polymer-specific language models while also overcoming the challenge of limited experimental polymer datasets. In PolyLLMem, the complementary information from both textual and structural domains was balanced, and a Low-rank adaptation (LoRA) layer was incorporated to fine-tune the embeddings with our target small polymer dataset during the property prediction tasks. We evaluated PolyLLMem on predictions of 22 polymer properties, and our results revealed that the integrated approach yields performance comparable to, and in some cases exceeds, that of graph-based models, as well as transformer-based models that typically require pretraining on millions of polymer samples. The PolyLLMem offers several advantages: (i) it delivers robust performance on a wide range of property prediction tasks even when trained on a small dataset; (ii) it does not require extensive dataset curation, processing, or additional pretraining on the polymer data; and (iii) it is both fast to train and straightforward to implement.

Method

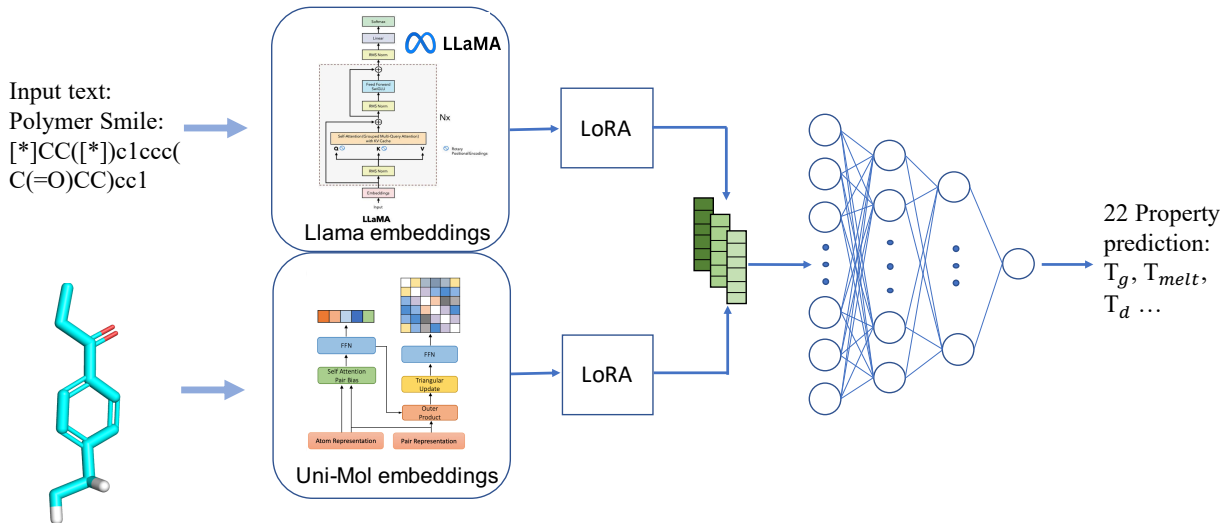


Figure 1. Schematic representation of PolyLLMem architecture. The architecture processes two inputs: text-based PSMILES string is encoded using the Llama 3 model to generate embeddings, while 3D molecular representations are processed by Uni-Mol to extract structural embeddings. These embeddings are merged after a LoRA layer to form a unified representation that is then employed in a single-task framework with a Multilayer Perceptron (MLP) for training and predicting polymer properties.

Data Collection

Our dataset comprises 29,639 data points of homopolymers covering 22 properties obtained from both DFT calculations and experimental measurements, sourced from peer-reviewed literatures and established databases.^{28,41-47} The properties, including glass transition temperature (T_g), melting temperature (T_m), thermal decomposition temperature (T_d), atomization energy (E_{at}), crystallization tendency (X_c), density (ρ), band gap (chain) (E_{gc}), band gap (bulk) (E_{gb}), electron affinity (E_{ea}), ionization energy (E_i), refractive index (n_c), conductivity (σ), tensile strength at yield (σ_y), Young’s modulus (E), tensile strength at break (σ_b), elongation at break (ϵ_b), and gas permeability of O₂, CO₂, N₂, H₂, He, CH₄ (μ_{O_2} , μ_{CO_2} , μ_{N_2} , μ_{H_2} , μ_{He} and μ_{CH_4}). The detailed distribution range for each property is provided in Table 1 and Supplementary Information (SI). Due to the extensive range observed in gas

permeability values, mechanical-related properties, and conductivity, which span several orders of magnitude, a base-10 logarithmic transformation was applied to μ_{O_2} , μ_{CO_2} , μ_{N_2} , μ_{H_2} , μ_{He} , μ_{CH_4} , σ_y , E , σ_b , ϵ_b and σ to normalize their distributions and stabilize the variance. Finally, the polymer dataset was split into training and testing sets using an 85/15 ratio, with the testing set reserved solely for final property prediction.

Table 1. Polymer property dataset with sources, data ranges, and data points. The data set contains 22 properties for homo polymers.

Property	Symbol	Unit	Source	Data Range	Data Points
Glass transition temp.	T_g	°C	Exp.	[-1.2e+02, 5e+02]	6769
Melting temp.	T_m	°C	Exp.	[-5.5e+01, 5.8e+02]	3349
Thermal decomposition temp.	T_d	°C	Exp.	[1.8e+01, 8.5e+02]	5347
Atomization energy	E_{at}	eV atom ⁻¹	DFT	[-7e+00, -5e+00]	390
Crystallization tendency (DFT)	X_c	%	DFT	[1e-01, 1e+02]	432
Density	ρ	g cm ⁻³	Exp.	[1e-01, 3e+00]	1520
Band gap (chain)	E_{gc}	eV	DFT	[2e-02, 1e+01]	3380
Band gap (bulk)	E_{gb}	eV	DFT	[4e-01, 1e+01]	561
Electron affinity	E_{ea}	eV	DFT	[4e-01, 5e+00]	368
Ionization energy	E_i	eV	DFT	[3.5e+00, 1e+01]	370
Refractive index	n_c	-	DFT	[1e+00, 3e+00]	382
Conductivity	σ	S/cm	Exp.	[0e+00, 1e+07]	382
Young’s modulus	E	GPa	Exp.	[2e-05, 6e+00]	938
Tensile strength at yield	σ_y	GPa	Exp.	[3e-08, 4e-01]	244
Tensile strength at break	σ_b	GPa	Exp.	[8e-05, 2e-01]	975
Elongation at break	ϵ_b	-	Exp.	[6e-01, 1e+03]	1015
O ₂ gas permeability	μ_{O_2}	barrer	Exp.	[3e-04, 1.9e+04]	695
CO ₂ gas permeability	μ_{CO_2}	barrer	Exp.	[1e-03, 4.7e+04]	644
N ₂ gas permeability	μ_{N_2}	barrer	Exp.	[1e-04, 1.7e+04]	678
H ₂ gas permeability	μ_{H_2}	barrer	Exp.	[2e-02, 3.7e+04]	461
He gas permeability	μ_{He}	barrer	Exp.	[5e-02, 1.8e+04]	408
CH ₄ gas permeability	μ_{CH_4}	barrer	Exp.	[4e-04, 3.5e+04]	331

Model Architecture

Our multimodal model (PolyLLMem) integrated LLM-based and Uni-Mol-based embeddings to predict polymer properties by capturing both textual and structural information. The LLM-based embeddings were generated using the LLM Llama 3 by mean pooling the final hidden states (token-level embeddings) to produce a single embedding vector with 4096 dimensions for each input textual string.³⁴ Each input string, as shown in Figure. 1 follows the format “Polymer Smile: PSMILES,” where PSMILES represent the polymer SMILES.

The mean pooling of the token-level embeddings effectively distills the rich chemical context captured by the LLM-based model into a robust representation.

In parallel, we employed Uni-Mol embeddings, which were 1536-dimensional, to capture the 3D geometry and conformational details of the molecules. This approach yielded embeddings that encapsulate critical geometric relationships, providing complementary structural insights to the text-based representations obtained from the Llama 3. Moreover, since Uni-Mol does not recognize PSMILES, we replaced the asterisk `*` with `"C"` in the input for Uni-Mol. Once both embeddings were obtained, each was projected into a common latent space with a predefined hidden size using a linear layer with Gaussian Error Linear Unit (GELU) activation and batch normalization. LoRA layers further refined these projections, and a gated fusion mechanism dynamically combines the updated LLM and Uni-Mol representations.⁴⁸ The fused embeddings are then processed through a refinement block and a regression network, which ultimately predicts the target polymer property. In our work, we focused on a single-property prediction task.

Training

Our training procedure employed 5-fold cross-validation to ensure a robust evaluation of the model’s predictive performance. Training was performed using the AdamW optimizer with a learning rate scheduler (ReduceLRonPlateau) and an early stopping mechanism was applied to prevent overfitting.^{49,50} Multiple loss functions, including Mean Square Error (MSE), Mean Absolute Error (MAE), and Huber, were used to guide optimization. For each fold, the best-performing model checkpoint was saved based on the validation loss, and final performance metrics (MAE and R^2) were computed on the test set and averaged across folds. Additionally, a grid search was used for hyperparameter tuning, optimizing key parameters such as hidden size, batch size, dropout rate, rank, alpha, learning rate, and weight decay.

For baseline comparisons, we evaluated a suite of classical ML models, including RF, Linear Regression, Support Vector Regression(SVR), Decision Tree, Ridge Regression, Ad-

aBoost, XGBoost, and a multilayer perceptron (MLP), using two distinct sets of input features separately: molecular descriptors (200 computed molecular properties) extracted from RDKit’s Descriptors.descList module, and Morgan fingerprints (MF) obtained from the RDKit package.²⁰ Additionally, for further comparison, embeddings generated by the Llama 3 and Uni-Mol were separately evaluated using classical ML models.

Discussions

To evaluate the feasibility of using the LLM embedding model for polymer property predictions, we employed two-dimensional Uniform Manifold Approximation and Projection (UMAP)⁵¹ to visualize the generated embeddings for all polymers in this study (see Figure 2). These embeddings were obtained by mean pooling the final layer of the Llama 3. In the UMAP plots, colored dots represent polymers with known property values for T_g (Figure 2a), T_d (Figure 2b), E_{gc} (Figure 2c) and E (Figure 2d), while light gray dots indicate polymers with unknown property values. In each plot, polymers with similar property values tend to form localized clusters of similar colors, with the exception of the E , where the differentiation was less distinct compared to the other properties. Nonetheless, this observation is noteworthy as it suggests that the LLM has successfully retained key chemical information and relationships inherent in the PSMILES strings, even though its predictive performance for properties like E may not be as robust as for others.

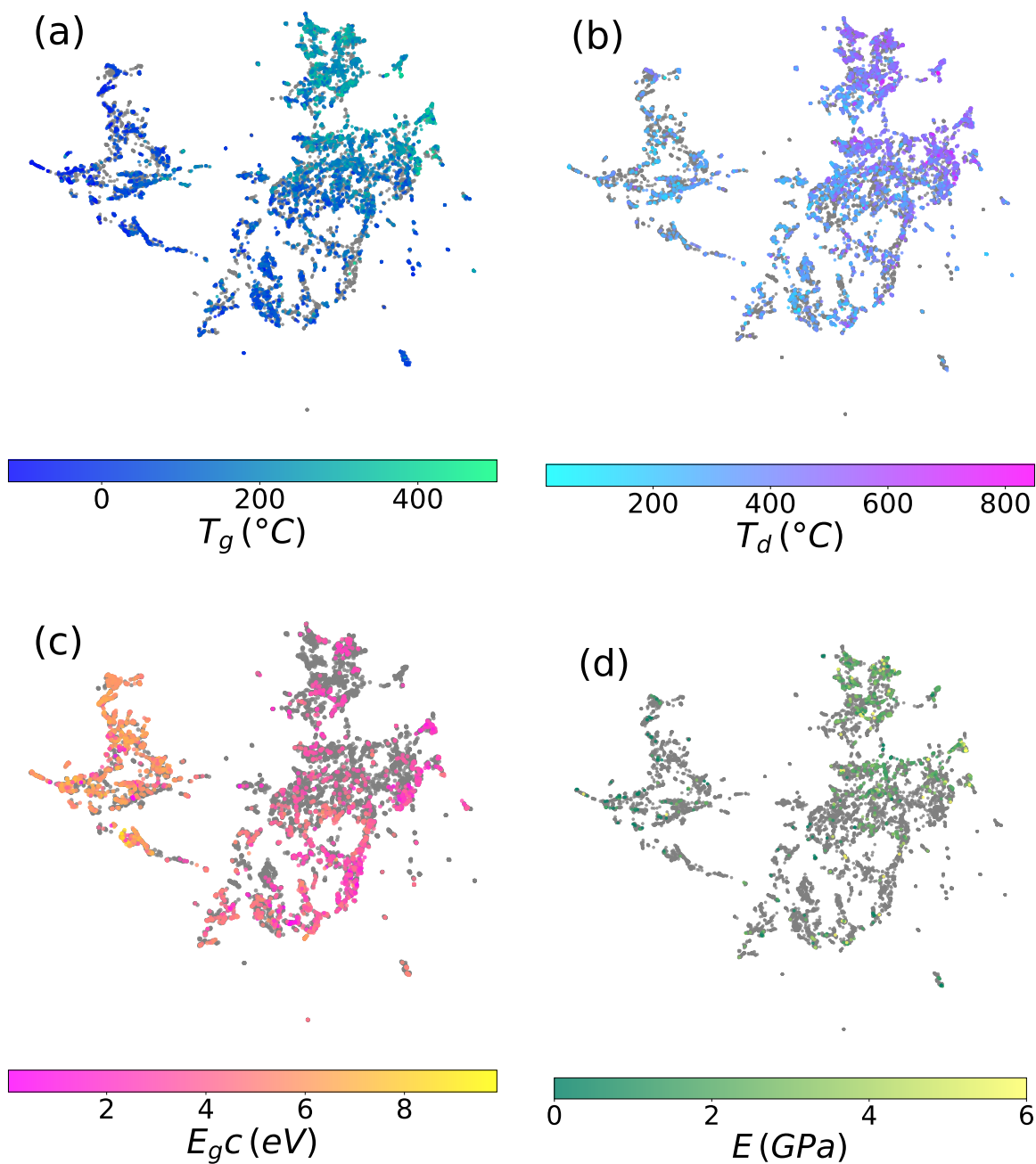


Figure 2. Two-dimensional Uniform Manifold Approximation and Projection (UMAP) plots of the embeddings generated from Llama 3 across all the polymers in this study. Panels (a–d) display colored dots representing property values for glass transition temperature (T_g), thermal decomposition temperature (T_d), chain band gap (E_{gc}), and Young’s modulus (E), respectively. Light gray dots indicate polymers with unknown property values.

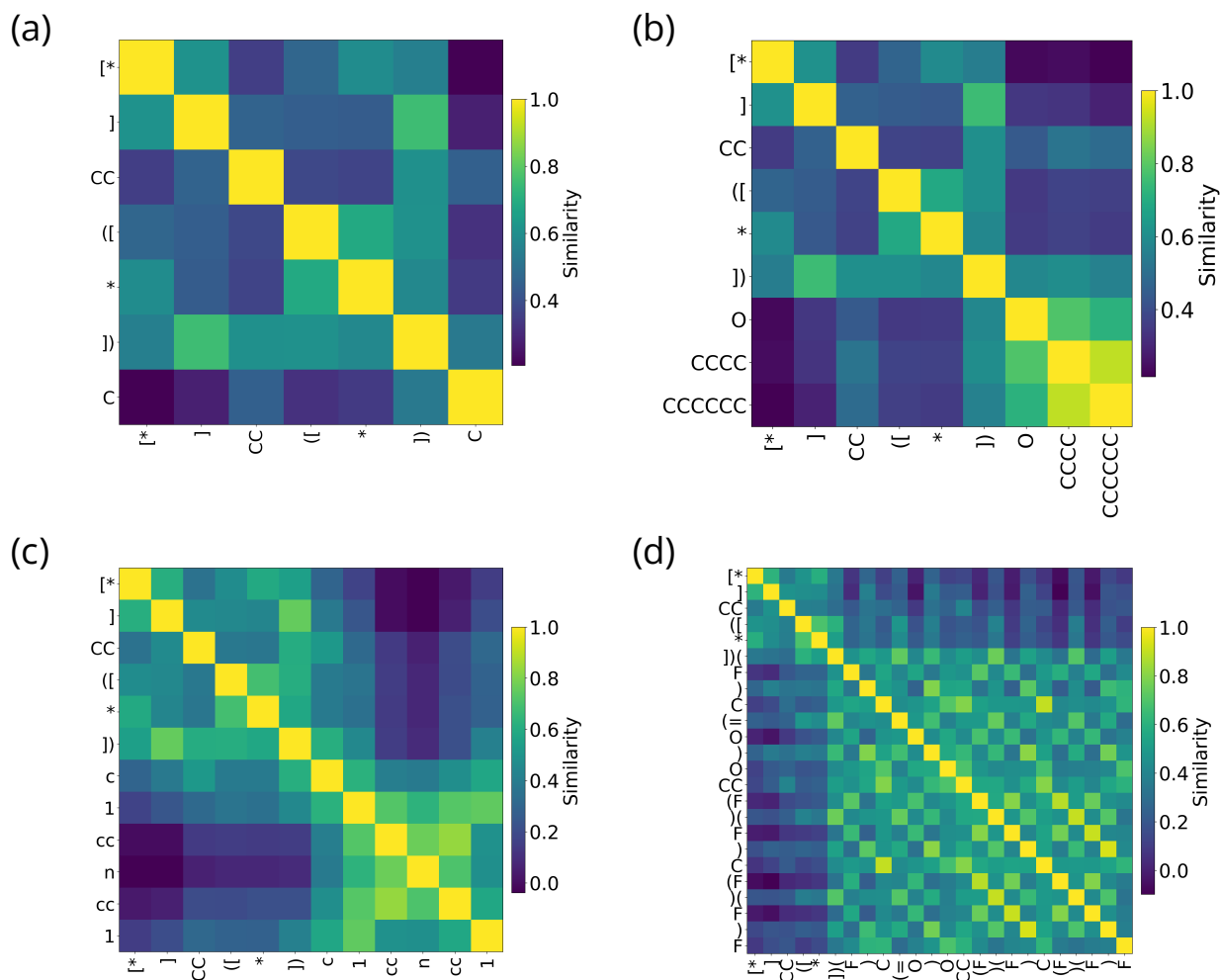


Figure 3. Cosine similarity was computed for the token-level embeddings of the selected polymers (a–d): [*]CC([*])C, [*]CC([*])OCCCCCCCCC, [*]CC([*])c1ccncc1, [*]CC([*])(F)C(=O)OCC(F)(F)C(F)(F)F. The resulting heatmaps display pairwise token similarities, with values near 1 indicating that tokens exhibit highly similar embedding representations, suggesting shared chemical or structural features.

To further explore the LLM’s ability to capture chemical information in polymers, we extracted token-level embeddings. Rather than using the embeddings after mean pooling for UMAP visualization, we retained the individual token representations prior to mean pooling to compute the cosine similarity across all tokens for the selected polymer. In all the panel Figure 3a-d, tokens used for polymer notation such as parentheses (,) or bracket placeholders [*], tend to have moderate similarity scores with each other, reflecting the model’s understanding of how they are used in PSMILES to denote branching, repeating units, or

unspecified substituents. In contrast, lower similarity scores appear between tokens that represent clearly different chemical entities or notational functions (e.g., tokens related to side chains vs. [*] tokens). This separation indicates that the embeddings capture meaningful distinctions in chemical context.

In Figure 3b, tokens corresponding to related chemical motifs, such as CCCC versus CCCCCC, show higher similarity scores, suggesting that the model recognizes these tokens as playing similar structural roles. Moreover, even among purely carbon tokens, subtle differences in length can lead to slightly different similarity scores. In Figure 3c, the PSMILES fragment consists of tokens such as c, 1, cc, n, cc, and 1, which collectively form a pyridine ring (e.g., c1ccncc1). These tokens show high inter-token similarity, indicating that the model recognizes them as parts of a unified aromatic ring structure and effectively captures their ring connectivity. In Figure 3d, the presence of clear clustering for fluorine tokens, along with the separation from purely carbon-based tokens, demonstrates the LLM’s ability to encode chemically relevant distinctions. Fluorine substituents have well-known effects on polymer properties (e.g., polarity, thermal stability), and the LLM embeddings’ separation of F from other tokens implies an internalized understanding of this difference. Overall, although the tokenizer used to train Llama may not perfectly differentiate certain aspects of polymer PSMILES (for instance, the tokens for [] and () are not distinctly separated), the LLM model still captures both syntactic and chemical relationships within PSMILES strings. While token-level embeddings retain considerably more information than mean-pooled embeddings, we opted for the aggregated embeddings for their simplicity and to demonstrate the effectiveness of the LLM embedding model in property prediction tasks.

After confirming that the LLM embeddings using Llama 3 retained essential chemical information, we evaluated their predictive performance on over 22 distinct polymer properties. Initially, the generated 4096-dimensional embeddings for each polymer were used as input to a XGBoost model (LLM+XGB).⁵² The performance results for various polymer properties were summarized in Table 1, which reports the average R^2 values obtained from five-fold

Table 2. Comparison of predictive performance (mean R^2 scores \pm standard deviation) across various polymer properties for different models. Results were obtained using five-fold cross-validation on test datasets. PolyLLMem refers to the multimodal model integrating LLM-generated text embeddings and Uni-Mol structural embeddings. LLM+XX and Uni-Mol+XX denote models utilizing embeddings from Llama 3 or Uni-Mol, respectively, as input features for the indicated methods (MLP, XGB). MF+XGB and Descriptors+XGB denote models using RDKit molecular fingerprints (MF) or RDKit molecular descriptors as input features for XGB. Best-performing results per property are highlighted in bold with arrows.

Property	PolyLLMem	LLM+MLP	Uni-Mol+MLP	LLM+XGB	Uni-Mol+XGB	MF+XGB	descriptors+XGB
ρ	0.83 \pm 0.03 \uparrow	0.70 \pm 0.06	0.74 \pm 0.05	0.58 \pm 0.02	0.67 \pm 0.03	0.62 \pm 0.02	0.73 \pm 0.05
T_g	0.89 \pm 0.01 \uparrow	0.88 \pm 0.01	0.85 \pm 0.01	0.84 \pm 0.00	0.82 \pm 0.01	0.87 \pm 0.00	0.87 \pm 0.00
T_m	0.77 \pm 0.01 \uparrow	0.75 \pm 0.02	0.70 \pm 0.01	0.70 \pm 0.01	0.63 \pm 0.01	0.76 \pm 0.01	0.68 \pm 0.02
T_d	0.73 \pm 0.01 \uparrow	0.66 \pm 0.01	0.63 \pm 0.04	0.66 \pm 0.02	0.59 \pm 0.01	0.72 \pm 0.01	0.71 \pm 0.01
σ_y	0.56 \pm 0.12	0.1 \pm 0.43	-0.43 \pm 0.32	-0.40 \pm 0.82	-0.83 \pm 1.51	0.60 \pm 0.17 \uparrow	0.12 \pm 0.39
σ_b	0.32 \pm 0.07 \uparrow	0.15 \pm 0.14	0.15 \pm 0.09	0.26 \pm 0.19	0.29 \pm 0.18	0.28 \pm 0.13	0.23 \pm 0.13
ϵ_b	0.24 \pm 0.04	0.19 \pm 0.08	0.04 \pm 0.10	0.32 \pm 0.05	0.31 \pm 0.04	0.34 \pm 0.04 \uparrow	0.10 \pm 0.08
E	0.52 \pm 0.06 \uparrow	0.37 \pm 0.05	0.40 \pm 0.05	0.43 \pm 0.07	0.28 \pm 0.07	0.46 \pm 0.03	0.34 \pm 0.13
σ	0.45 \pm 0.05	0.35 \pm 0.04	0.35 \pm 0.08	0.40 \pm 0.04	0.33 \pm 0.04	0.44 \pm 0.03	0.48 \pm 0.02 \uparrow
E_{gc}	0.92 \pm 0.01 \uparrow	0.88 \pm 0.01	0.88 \pm 0.01	0.81 \pm 0.01	0.80 \pm 0.02	0.86 \pm 0.01	0.88 \pm 0.01
X_c	0.40 \pm 0.03	0.44 \pm 0.03 \uparrow	0.27 \pm 0.09	0.37 \pm 0.06	0.26 \pm 0.08	0.28 \pm 0.08	0.31 \pm 0.05
E_{gb}	0.94 \pm 0.01 \uparrow	0.90 \pm 0.01	0.93 \pm 0.02	0.84 \pm 0.02	0.85 \pm 0.03	0.85 \pm 0.01	0.91 \pm 0.01
E_{at}	0.96 \pm 0.02 \uparrow	0.90 \pm 0.03	0.90 \pm 0.02	0.74 \pm 0.07	0.80 \pm 0.02	0.81 \pm 0.03	0.90 \pm 0.02
E_{ca}	0.92 \pm 0.01 \uparrow	0.86 \pm 0.02	0.91 \pm 0.02	0.63 \pm 0.07	0.75 \pm 0.03	0.83 \pm 0.02	0.79 \pm 0.02
E_i	0.81 \pm 0.04 \uparrow	0.76 \pm 0.05	0.75 \pm 0.03	0.70 \pm 0.05	0.62 \pm 0.04	0.76 \pm 0.03	0.69 \pm 0.05
n_c	0.83 \pm 0.01 \uparrow	0.72 \pm 0.11	0.72 \pm 0.02	0.69 \pm 0.03	0.69 \pm 0.04	0.69 \pm 0.06	0.82 \pm 0.03
μ_{CO_2}	0.83 \pm 0.02 \uparrow	0.76 \pm 0.06	0.63 \pm 0.12	0.73 \pm 0.03	0.64 \pm 0.05	0.73 \pm 0.04	0.74 \pm 0.03
μ_{H_2}	0.85 \pm 0.03 \uparrow	0.80 \pm 0.04	0.81 \pm 0.03	0.81 \pm 0.03	0.66 \pm 0.05	0.85 \pm 0.04	0.79 \pm 0.03
μ_{CH_4}	0.87 \pm 0.03 \uparrow	0.79 \pm 0.01	0.84 \pm 0.02	0.78 \pm 0.05	0.72 \pm 0.05	0.81 \pm 0.03	0.80 \pm 0.01
μ_{He}	0.81 \pm 0.02 \uparrow	0.76 \pm 0.04	0.74 \pm 0.03	0.77 \pm 0.04	0.65 \pm 0.07	0.77 \pm 0.01	0.65 \pm 0.05
μ_{N_2}	0.79 \pm 0.01 \uparrow	0.79 \pm 0.02	0.68 \pm 0.08	0.61 \pm 0.05	0.67 \pm 0.02	0.78 \pm 0.02	0.70 \pm 0.03
μ_{O_2}	0.87 \pm 0.01 \uparrow	0.86 \pm 0.03	0.77 \pm 0.06	0.75 \pm 0.03	0.66 \pm 0.04	0.78 \pm 0.04	0.69 \pm 0.04

cross-validation on the test set. LLM+XGB achieved good performance on several polymer properties, with T_g , E_{gc} , E_{gb} , μ_{H_2} , each exhibiting R^2 value above 0.8. These results support our UMAP analysis, indicating that the LLM embeddings capture meaningful chemical information and perform well on certain properties prediction tasks. However, when compared with benchmark models trained on MF features (MF+XGB) or molecular descriptors (descriptors+XGB), LLM+XGB consistently underperformed across most property predictions, particularly when contrasted with MF+XGB. In addition, we evaluated other ML models such as RF, Ridge Regression, AdaBoost, MLP, etc. using the LLM-generated embeddings. Among these, the model combining LLM embeddings with an MLP (LLM+MLP) demonstrated exceptional performance, yielding results that were comparable to those of the benchmark models on the majority of the property prediction tasks, as shown in Table 1. Additional results for other models were provided in the SI, as their performances were inferior to those of the benchmark models. We also trained MLP models using MF features and molecular descriptors respectively, but these results were inferior to those obtained with MF+XGB or descriptors+XGB (details were provided in the SI). Moreover, Uni-Mol embeddings alone as input features for ML models were shown in Table 1 as comparison.

Although LLM+MLP demonstrated exceptional performance overall, there remains room for improvement since the gains in prediction accuracy were modest and some property prediction tasks still underperformed compared to the baseline models. LLM based embeddings primarily capture textual information from PSMILES strings, leaving out crucial aspects of a molecule’s structure. To address this gap, we introduced Uni-Mol, a deep learning architecture that encodes the 3D geometry and conformational characteristics of small molecules, to generate embeddings that capture structural information, and integrated them with LLM-based embeddings to form the multimodal model PolyLLMem. As shown in Table 1, PolyLLMem demonstrated superior performance on most property prediction tasks compared to the baseline models, except for certain mechanical properties (σ_y , ϵ_b), crystallization tendency X_c and conductivity σ . Additionally, we compared the prediction

results of PolyLLMem with those of other graph-based and transformer-based models, such as PolymerBERT, TransPolymer, and PolyGNN, as detailed in the SI. Given the limited training data used in our study, PolyLLMem exhibits performance that is comparable to, and in some cases exceeds, that of these benchmark models on the majority of polymer properties. However, PolyLLMem’s performance in predicting gas permeability was not as competitive as that of the graph-based and transformer-based models. Several factors may contribute to this discrepancy. One potential factor is that the training dataset may have introduced differences. We used the latest experimental gas permeability data from Phan et al.,⁴⁷ which is more diverse than the data used to train PolymerBERT and PolyGNN in their original studies. In fact, even for a single-task prediction, PolyGNN’s performance with this new dataset in their latest work⁴⁷ was lower than reported in its original paper.²⁸ Moreover, PolymerBERT employed multitask training, which may enable it to capture a broader range of information compared to our single-task approach, resulting in improved performance for certain properties. Additionally, our findings indicate that PolyLLMem struggled to accurately predict mechanical properties, suggesting that further model refinement or additional data may be necessary to enhance its performance in this area.

Lastly, we evaluated the interpretability of the model. In our model, we extracted the token-level embeddings and applied a mean pooling layer to obtain the aggregated representation used by PolyLLMem. Using this setup, we computed Integrated Gradients⁵³ along the path from a zero (baseline) input to the actual token-level embeddings by passing them through a wrapper function that performs the mean pooling, thereby generating token-level attributions. By analyzing the aggregated attribution values for each token, we identified those that contributed most significantly to the predictions. Figure 4 shows the token attributions for T_g prediction from the selected polymers. For polymer [*]CC([*])C in Figure 4a, the tokens representing the carbon backbone (CC) and the polymerization point tokens ([*]) show relatively high aggregated attribution values, indicating that the model emphasizes the alkyl backbone and its connection points. In Figure 4b, for polymer [*]CC([*])c1ccncc1,

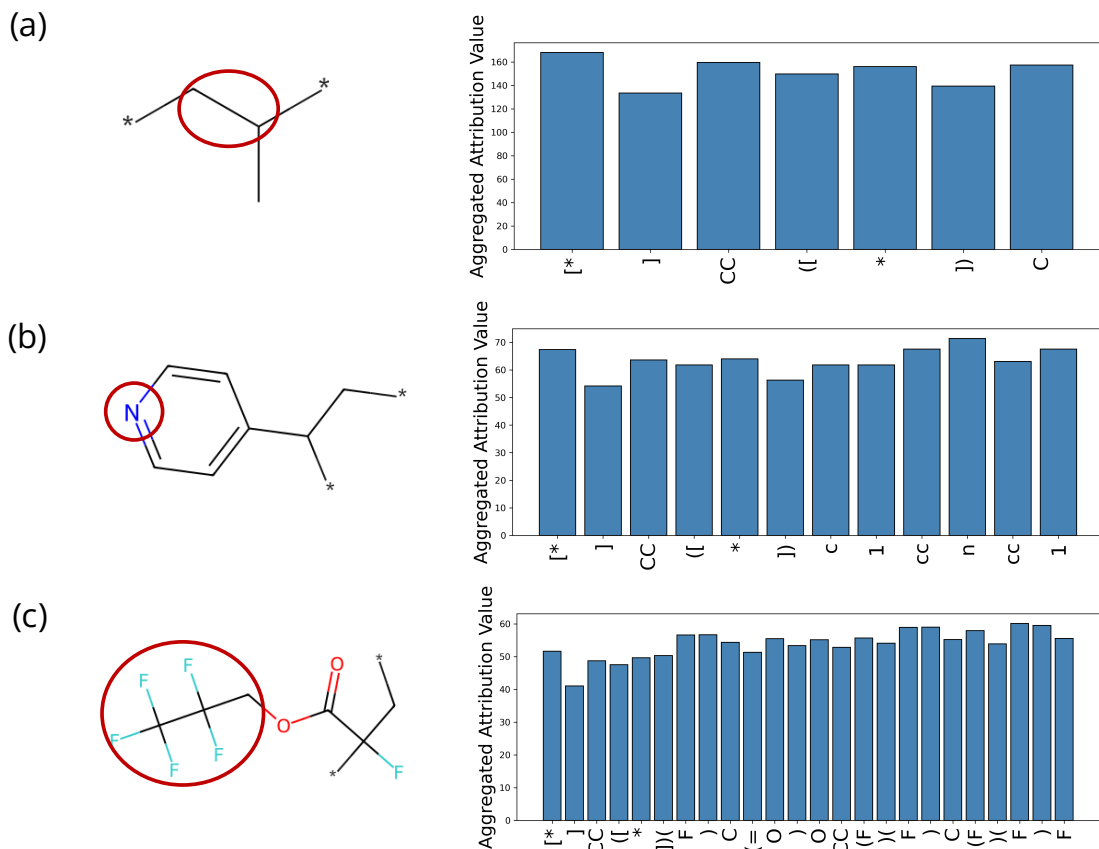


Figure 4. Token-level attribution analysis for T_g prediction using PolyLLMem of selected polymers: (a) [*]CC([*])C, (b) [*]CC([*])c1ccncc1, (c) [*]CC([*])(F)C(=O)OCC(F)(F)C(F)(F)F. Token level attributions were computed using Integrated Gradients, highlighting the contribution of individual chemical tokens to model predictions. High attribution values indicate greater significance in determining the predicted property. Red circles are used to label the atoms that have the highest attributions

the tokens corresponding to the nitrogen containing ring (`n`) as highlighted by the red marker, and the ring closure marker (`1`) exhibit higher aggregated attribution values, suggesting that the model focuses on these structural features. In polymer chemistry, heteroaromatic rings, particularly those containing nitrogen, can significantly affect chain packing and polarity, which in turn affects T_g . Lastly, in polymer [*]CC([*])(F)C(=O)OCC(F)(F)C(F)(F)F, which exhibits one of the highest T_g values in our dataset, the tokens corresponding to the trifluoromethyl ($-\text{CF}_3$) groups have the highest aggregated attribution values, suggesting the model strongly focuses on these fluorinated groups. This also aligns with real world polymer chemistry, where fluorinated groups can significantly affect chain rigidity and consequently

increase T_g . Collectively, the model’s attention to these functional groups and structural moieties demonstrates its ability to capture the key chemical features that determine T_g in practice.

Conclusion

In this study, we introduced a simple yet effective multimodal framework, PolyLLMem, which synergistically integrates LLM-based text embeddings with 3D molecular structure embeddings from Uni-Mol to predict a wide range of polymer properties. By leveraging PSMILES strings as a source of rich textual information and integrating them with geometrical descriptors, our approach successfully encapsulates both the chemical context inherent in polymer notations and the critical conformational features of polymer molecules. Our extensive evaluation across 22 distinct property prediction tasks demonstrated that PolyLLMem achieves competitive performance compared to established transformer and graph-based models that are specifically designed for the polymer domain. Remarkably, while those models, especially transformer-based models, typically require training on millions of data points, our model was developed using a relatively small dataset, underscoring its simplicity and effectiveness. Notably, the LLM embeddings model alone (LLM+XGB) showed promise for properties such as T_g , E_{gc} , and E_{gb} , indicating some of the chemical information within polymer domains already embedded in the LLM. To integrate the LLM embeddings model with 3D structural information further enhanced predictive accuracy across most tasks. Additionally, using Integrated Gradients also revealed that the model effectively identifies key chemical motifs and structural features in line with established chemical intuition.

Despite these promising results, challenges remain, particularly in predicting certain mechanical properties. These discrepancies highlight the inherent complexities of polymer data and indicate the need for further refinement of data augmentation techniques and model architectures. Future work could enhance the embedding model’s complexity by leveraging

token-level embeddings in conjunction with multi-head attention mechanisms, which may further improve the accuracy of polymer property predictions. Overall, our work underscores the potential of combining LLM embeddings with molecular structure information to accelerate the discovery and optimization of polymer materials.

Code availability

The PolyLLMem code is available for academic use at <https://github.com/zhangtr10/PolyLLMem>.

Conflict of Interest

The authors have no conflicts to disclose.

Acknowledgement

This work employed Jetstream2 through allocation TG-MAT250013 from the Advanced Cyberinfrastructure Coordination Ecosystem, Services & Support (ACCESS) and Delaware Advanced Research Workforce and Innovation Network (DARWIN).

References

- (1) Ornaghi Jr, H. L.; Monticeli, F. M.; Agnol, L. D. A Review on Polymers for Biomedical Applications on Hard and Soft Tissues and Prosthetic Limbs. *Polymers* **2023**, *15*, 4034.
- (2) Oladele, I. O.; Omotosho, T. F.; Adediran, A. A. Polymer-based composites: an indispensable material for present and future applications. *International Journal of Polymer Science* **2020**, *2020*, 8834518.
- (3) Doan Tran, H.; Kim, C.; Chen, L.; Chandrasekaran, A.; Batra, R.; Venkatram, S.; Kamal, D.; Lightstone, J. P.; Gurnani, R.; Shetty, P.; others Machine-learning predictions of polymer properties with Polymer Genome. *Journal of Applied Physics* **2020**, *128*.

- (4) McDonald, S. M.; Augustine, E. K.; Lanners, Q.; Rudin, C.; Catherine Brinson, L.; Becker, M. L. Applied machine learning as a driver for polymeric biomaterials design. *Nature Communications* **2023**, *14*, 4838.
- (5) Sharma, A.; Mukhopadhyay, T.; Rangappa, S. M.; Siengchin, S.; Kushvaha, V. Advances in computational intelligence of polymer composite materials: machine learning assisted modeling, analysis and design. *Archives of Computational Methods in Engineering* **2022**, *29*, 3341–3385.
- (6) Xu, P.; Chen, H.; Li, M.; Lu, W. New opportunity: machine learning for polymer materials design and discovery. *Advanced Theory and Simulations* **2022**, *5*, 2100565.
- (7) Ge, W.; De Silva, R.; Fan, Y.; Sisson, S. A.; Stenzel, M. H. Machine Learning in Polymer Research. *Advanced Materials* **2025**, 2413695.
- (8) Patra, T. K. Data-driven methods for accelerating polymer design. *ACS Polymers Au* **2021**, *2*, 8–26.
- (9) Weininger, D. SMILES, a chemical language and information system. 1. Introduction to methodology and encoding rules. *Journal of Chemical Information and Computer Sciences* **1988**, *28*, 31–36.
- (10) Lin, T.-S.; Coley, C. W.; Mochigase, H.; Beech, H. K.; Wang, W.; Wang, Z.; Woods, E.; Craig, S. L.; Johnson, J. A.; Kalow, J. A.; others BigSMILES: a structurally-based line notation for describing macromolecules. *ACS central science* **2019**, *5*, 1523–1531.
- (11) Kuenneth, C.; Ramprasad, R. polyBERT: a chemical language model to enable fully machine-driven ultrafast polymer informatics. *Nature communications* **2023**, *14*, 4099.
- (12) Kim, C.; Chandrasekaran, A.; Huan, T. D.; Das, D.; Ramprasad, R. Polymer genome: a data-powered polymer informatics platform for property predictions. *The Journal of Physical Chemistry C* **2018**, *122*, 17575–17585.

- (13) Tao, L.; Varshney, V.; Li, Y. Benchmarking machine learning models for polymer informatics: an example of glass transition temperature. *Journal of Chemical Information and Modeling* **2021**, *61*, 5395–5413.
- (14) Wu, S.; Kondo, Y.; Kakimoto, M.-a.; Yang, B.; Yamada, H.; Kuwajima, I.; Lambert, G.; Hongo, K.; Xu, Y.; Shiomi, J.; others Machine-learning-assisted discovery of polymers with high thermal conductivity using a molecular design algorithm. *Npj Computational Materials* **2019**, *5*, 66.
- (15) Qiu, H.; Liu, L.; Qiu, X.; Dai, X.; Ji, X.; Sun, Z.-Y. PolyNC: a natural and chemical language model for the prediction of unified polymer properties. *Chemical Science* **2024**, *15*, 534–544.
- (16) Uddin, M. J.; Fan, J. Interpretable machine learning framework to predict the glass transition temperature of polymers. *Polymers* **2024**, *16*, 1049.
- (17) Zhao, Y.; Mulder, R. J.; Houshyar, S.; Le, T. C. A review on the application of molecular descriptors and machine learning in polymer design. *Polymer Chemistry* **2023**, *14*, 3325–3346.
- (18) Ma, R.; Luo, T. PI1M: a benchmark database for polymer informatics. *Journal of Chemical Information and Modeling* **2020**, *60*, 4684–4690.
- (19) Volgin, I. V.; Batyr, P. A.; Matseevich, A. V.; Dobrovskiy, A. Y.; Andreeva, M. V.; Nazarychev, V. M.; Larin, S. V.; Goikhman, M. Y.; Vizilter, Y. V.; Askadskii, A. A.; others Machine learning with enormous “synthetic” data sets: predicting glass transition temperature of polyimides using graph convolutional neural networks. *ACS omega* **2022**, *7*, 43678–43691.
- (20) Landrum, G.; others RDKit: A software suite for cheminformatics, computational chemistry, and predictive modeling. *Greg Landrum* **2013**, *8*, 5281.

- (21) Rogers, D.; Hahn, M. Extended-connectivity fingerprints. *Journal of chemical information and modeling* **2010**, *50*, 742–754.
- (22) Gilmer, J.; Schoenholz, S. S.; Riley, P. F.; Vinyals, O.; Dahl, G. E. Neural message passing for quantum chemistry. International conference on machine learning. 2017; pp 1263–1272.
- (23) Wilson, A. N.; St John, P. C.; Marin, D. H.; Hoyt, C. B.; Rognerud, E. G.; Nimlos, M. R.; Cywar, R. M.; Rorrer, N. A.; Shebek, K. M.; Broadbelt, L. J.; others PolyID: Artificial intelligence for discovering performance-advantaged and sustainable polymers. *Macromolecules* **2023**, *56*, 8547–8557.
- (24) Yue, T.; He, J.; Tao, L.; Li, Y. High-throughput screening and prediction of high modulus of resilience polymers using explainable machine learning. *Journal of Chemical Theory and Computation* **2023**, *19*, 4641–4653.
- (25) Tao, L.; He, J.; Munyaneza, N. E.; Varshney, V.; Chen, W.; Liu, G.; Li, Y. Discovery of multi-functional polyimides through high-throughput screening using explainable machine learning. *Chemical Engineering Journal* **2023**, *465*, 142949.
- (26) Zeng, M.; Kumar, J. N.; Zeng, Z.; Savitha, R.; Chandrasekhar, V. R.; Hippalgaonkar, K. Graph convolutional neural networks for polymers property prediction. *arXiv preprint arXiv:1811.06231* **2018**,
- (27) Huang, Q.; Chen, Z.; Lin, Z.; Li, W.; Yu, W.; Zhu, L. Enhancing copolymer property prediction through the weighted-chained-SMILES machine learning framework. *ACS Applied Polymer Materials* **2024**, *6*, 3666–3675.
- (28) Gurnani, R.; Kuenneth, C.; Toland, A.; Ramprasad, R. Polymer informatics at scale with multitask graph neural networks. *Chemistry of Materials* **2023**, *35*, 1560–1567.

- (29) Xu, C.; Wang, Y.; Barati Farimani, A. TransPolymer: a Transformer-based language model for polymer property predictions. *npj Computational Materials* **2023**, *9*, 64.
- (30) Zhang, P.; Kearney, L.; Bhowmik, D.; Fox, Z.; Naskar, A. K.; Gounley, J. Transferring a molecular foundation model for polymer property predictions. *Journal of Chemical Information and Modeling* **2023**, *63*, 7689–7698.
- (31) Chithrananda, S.; Grand, G.; Ramsundar, B. ChemBERTa: large-scale self-supervised pretraining for molecular property prediction. *arXiv preprint arXiv:2010.09885* **2020**,
- (32) Wang, F.; Guo, W.; Cheng, M.; Yuan, S.; Xu, H.; Gao, Z. Mmpolymer: A multimodal multitask pretraining framework for polymer property prediction. Proceedings of the 33rd ACM International Conference on Information and Knowledge Management. 2024; pp 2336–2346.
- (33) Achiam, J.; Adler, S.; Agarwal, S.; Ahmad, L.; Akkaya, I.; Aleman, F. L.; Almeida, D.; Altenschmidt, J.; Altman, S.; Anadkat, S.; others Gpt-4 technical report. *arXiv preprint arXiv:2303.08774* **2023**,
- (34) Grattafiori, A.; Dubey, A.; Jauhri, A.; Pandey, A.; Kadian, A.; Al-Dahle, A.; Letman, A.; Mathur, A.; Schelten, A.; Vaughan, A.; others The llama 3 herd of models. *arXiv preprint arXiv:2407.21783* **2024**,
- (35) Touvron, H.; Lavril, T.; Izacard, G.; Martinet, X.; Lachaux, M.-A.; Lacroix, T.; Rozière, B.; Goyal, N.; Hambro, E.; Azhar, F.; others Llama: Open and efficient foundation language models. *arXiv preprint arXiv:2302.13971* **2023**,
- (36) Jia, S.; Zhang, C.; Fung, V. Llm4design: Autonomous materials discovery with large language models. *arXiv preprint arXiv:2406.13163* **2024**,
- (37) Luu, R. K.; Buehler, M. J. BioinspiredLLM: Conversational large language model for

- the mechanics of biological and bio-inspired materials. *Advanced Science* **2024**, *11*, 2306724.
- (38) Stewart, I.; Buehler, M. Molecular analysis and design using multimodal generative artificial intelligence via multi-agent modeling. **2024**,
- (39) Chen, Y.; Zou, J. Simple and effective embedding model for single-cell biology built from ChatGPT. *Nature Biomedical Engineering* **2024**, 1–11.
- (40) Zhou, G.; Gao, Z.; Ding, Q.; Zheng, H.; Xu, H.; Wei, Z.; Zhang, L.; Ke, G. Uni-mol: A universal 3d molecular representation learning framework. **2023**,
- (41) Huan, T. D.; Mannodi-Kanakkithodi, A.; Ramprasad, R. Accelerated materials property predictions and design using motif-based fingerprints. *Physical Review B* **2015**, *92*, 014106.
- (42) Huan, T. D.; Mannodi-Kanakkithodi, A.; Kim, C.; Sharma, V.; Pilia, G.; Ramprasad, R. A polymer dataset for accelerated property prediction and design. *Scientific data* **2016**, *3*, 1–10.
- (43) Sharma, V.; Wang, C.; Lorenzini, R. G.; Ma, R.; Zhu, Q.; Sinkovits, D. W.; Pilia, G.; Oganov, A. R.; Kumar, S.; Sotzing, G. A.; others Rational design of all organic polymer dielectrics. *Nature communications* **2014**, *5*, 4845.
- (44) Otsuka, S.; Kuwajima, I.; Hosoya, J.; Xu, Y.; Yamazaki, M. PoLyInfo: Polymer database for polymeric materials design. 2011 International Conference on Emerging Intelligent Data and Web Technologies. 2011; pp 22–29.
- (45) Afzal, M. A. F.; Browning, A. R.; Goldberg, A.; Halls, M. D.; Gavartin, J. L.; Morisato, T.; Hughes, T. F.; Giesen, D. J.; Goose, J. E. High-throughput molecular dynamics simulations and validation of thermophysical properties of polymers for various applications. *ACS Applied Polymer Materials* **2020**, *3*, 620–630.

- (46) Kuenneth, C.; Rajan, A. C.; Tran, H.; Chen, L.; Kim, C.; Ramprasad, R. Polymer informatics with multi-task learning. *Patterns* **2021**, *2*.
- (47) Phan, B. K.; Shen, K.-H.; Gurnani, R.; Tran, H.; Lively, R.; Ramprasad, R. Gas permeability, diffusivity, and solubility in polymers: Simulation-experiment data fusion and multi-task machine learning. *npj Computational Materials* **2024**, *10*, 186.
- (48) Hu, E. J.; Shen, Y.; Wallis, P.; Allen-Zhu, Z.; Li, Y.; Wang, S.; Wang, L.; Chen, W.; others Lora: Low-rank adaptation of large language models. *ICLR* **2022**, *1*, 3.
- (49) Loshchilov, I.; Hutter, F. Decoupled weight decay regularization. *arXiv preprint arXiv:1711.05101* **2017**,
- (50) Pedregosa, F.; Varoquaux, G.; Gramfort, A.; Michel, V.; Thirion, B.; Grisel, O.; Blondel, M.; Prettenhofer, P.; Weiss, R.; Dubourg, V.; others Scikit-learn: Machine learning in Python. *Journal of machine learning research* **2011**, *12*, 2825–2830.
- (51) McInnes, L.; Healy, J.; Melville, J. Umap: Uniform manifold approximation and projection for dimension reduction. *arXiv preprint arXiv:1802.03426* **2018**,
- (52) Chen, T.; Guestrin, C. Xgboost: A scalable tree boosting system. Proceedings of the 22nd acm sigkdd international conference on knowledge discovery and data mining. 2016; pp 785–794.
- (53) Sundararajan, M.; Taly, A.; Yan, Q. Axiomatic attribution for deep networks. International conference on machine learning. 2017; pp 3319–3328.

Supporting Information Available

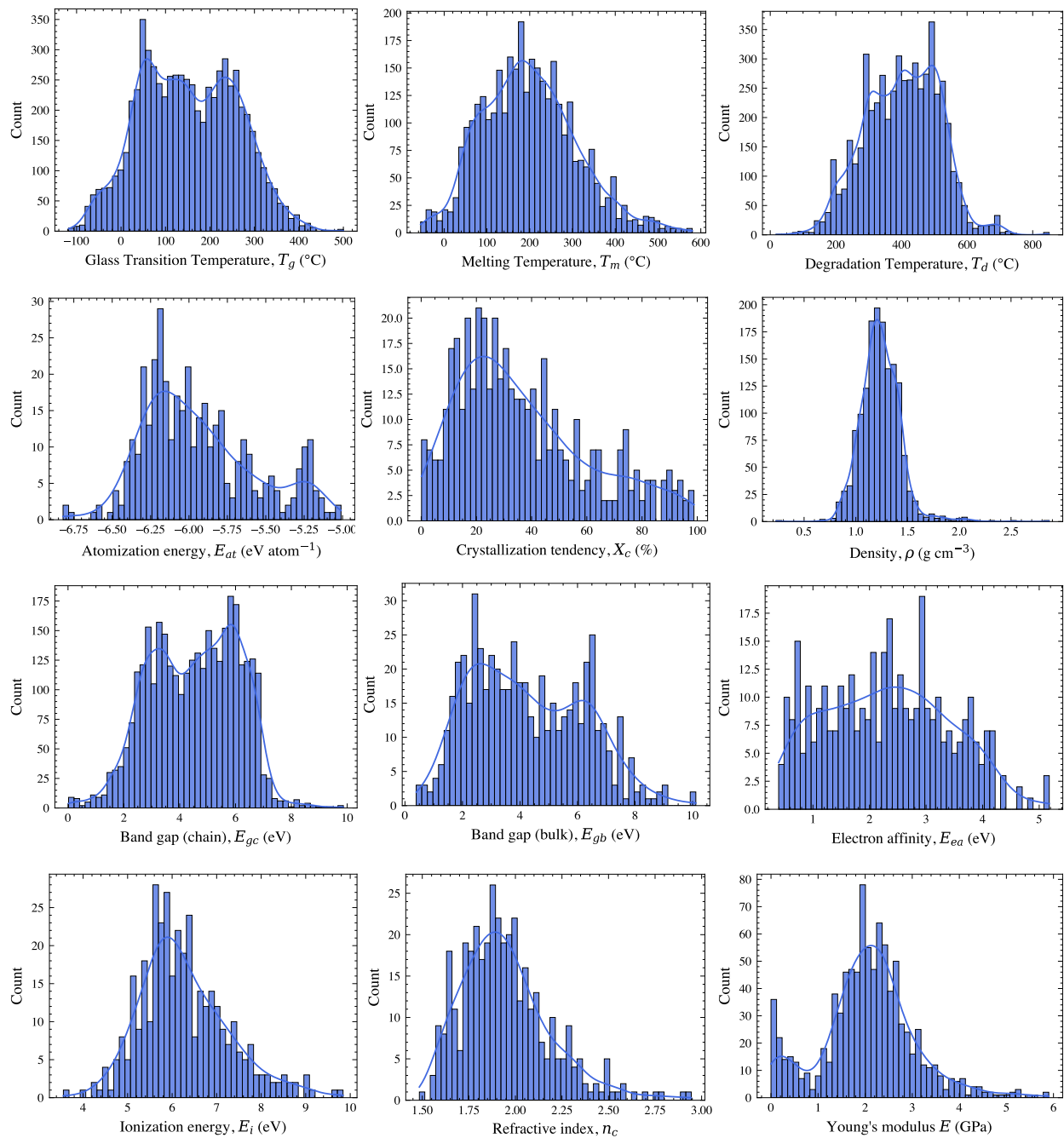


Figure 5. Figure S1a. Caption for subfigure (a).

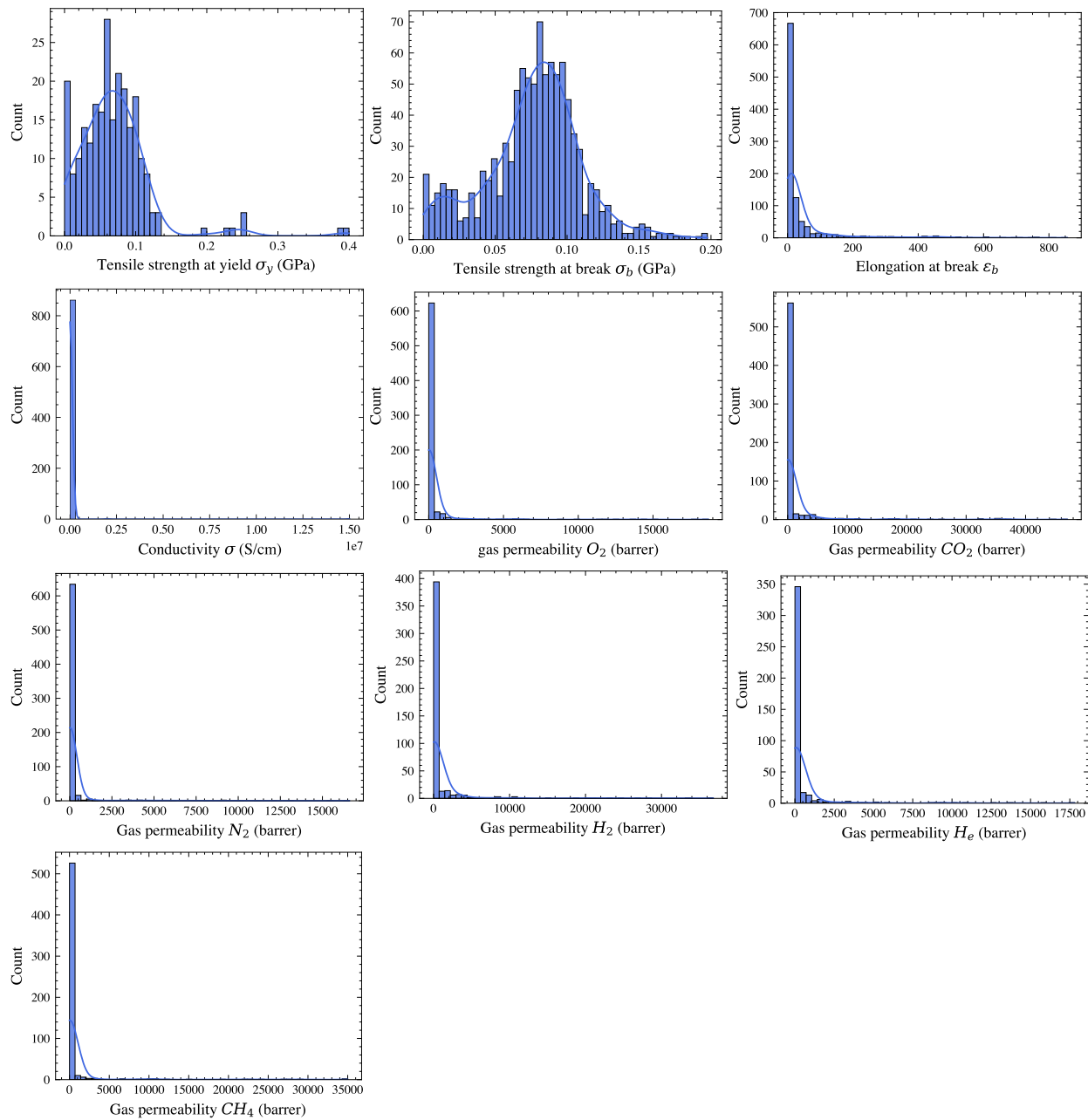


Figure S1. The detailed distribution range for each property.

Table S1. Comparison of predictive performance (R^2 scores \pm standard deviation) for polymer properties across various machine learning models using the embeddings generated from Llama 3 as input features.

Property	RandomForest	LinearRegression	SVR	DecisionTree	RidgeRegression	AdaBoost	GradientBoosting	XGBoost
ρ	0.51 \pm 0.02	0.60 \pm 0.06	0.61 \pm 0.01	0.27 \pm 0.13	0.65 \pm 0.05	0.43 \pm 0.02	0.60 \pm 0.02	0.58 \pm 0.02
T_g	0.82 \pm 0.00	0.77 \pm 0.02	0.63 \pm 0.00	0.63 \pm 0.02	0.76 \pm 0.02	0.73 \pm 0.00	0.82 \pm 0.00	0.84 \pm 0.00
T_m	0.67 \pm 0.02	0.37 \pm 0.05	0.30 \pm 0.00	0.37 \pm 0.09	0.52 \pm 0.03	0.60 \pm 0.01	0.70 \pm 0.01	0.70 \pm 0.01
T_d	0.61 \pm 0.01	0.20 \pm 0.02	0.42 \pm 0.00	0.28 \pm 0.05	0.32 \pm 0.03	0.51 \pm 0.01	0.60 \pm 0.01	0.66 \pm 0.02
σ_y	-0.18 \pm 0.45	-3.50 \pm 1.54	0.35 \pm 0.01	-5.20 \pm 2.72	-1.99 \pm 0.86	0.52 \pm 0.04	0.02 \pm 0.38	-5.01 \pm 0.36
σ_b	0.32 \pm 0.08	-0.67 \pm 0.13	0.23 \pm 0.01	-0.24 \pm 0.57	0.06 \pm 0.12	0.25 \pm 0.07	0.19 \pm 0.27	0.26 \pm 0.19
ϵ_b	0.36 \pm 0.06	-0.69 \pm 0.33	0.33 \pm 0.01	-0.44 \pm 0.06	0.06 \pm 0.12	0.33 \pm 0.03	0.39 \pm 0.04	0.32 \pm 0.05
E	0.45 \pm 0.09	-0.59 \pm 0.21	0.22 \pm 0.03	-0.51 \pm 0.29	0.06 \pm 0.14	0.43 \pm 0.03	0.45 \pm 0.05	0.43 \pm 0.07
σ	0.37 \pm 0.05	0.08 \pm 0.12	0.09 \pm 0.01	0.09 \pm 0.11	0.28 \pm 0.07	0.38 \pm 0.01	0.47 \pm 0.01	0.40 \pm 0.04
E_{gc}	0.78 \pm 0.01	0.70 \pm 0.02	0.85 \pm 0.00	0.59 \pm 0.02	0.76 \pm 0.02	0.73 \pm 0.01	0.80 \pm 0.00	0.81 \pm 0.01
X_c	0.39 \pm 0.04	-1.06 \pm 0.31	0.00 \pm 0.02	-0.12 \pm 0.17	-0.48 \pm 0.08	0.44 \pm 0.03	0.45 \pm 0.03	0.37 \pm 0.06
E_{gb}	0.81 \pm 0.02	0.82 \pm 0.02	0.85 \pm 0.01	0.49 \pm 0.09	0.86 \pm 0.02	0.84 \pm 0.01	0.86 \pm 0.01	0.84 \pm 0.02
E_{at}	0.72 \pm 0.04	0.90 \pm 0.03	0.83 \pm 0.03	0.50 \pm 0.06	0.90 \pm 0.03	0.78 \pm 0.02	0.81 \pm 0.02	0.74 \pm 0.07
E_{ea}	0.66 \pm 0.05	0.68 \pm 0.13	0.79 \pm 0.01	0.43 \pm 0.13	0.78 \pm 0.07	0.75 \pm 0.02	0.77 \pm 0.04	0.63 \pm 0.07
E_i	0.73 \pm 0.02	0.55 \pm 0.05	0.80 \pm 0.02	0.33 \pm 0.11	0.61 \pm 0.03	0.72 \pm 0.02	0.77 \pm 0.03	0.70 \pm 0.05
n_c	0.70 \pm 0.02	0.38 \pm 0.28	0.71 \pm 0.04	0.49 \pm 0.07	0.60 \pm 0.13	0.72 \pm 0.03	0.71 \pm 0.04	0.69 \pm 0.03
μ_{CO_2}	0.71 \pm 0.02	0.76 \pm 0.02	0.81 \pm 0.01	0.41 \pm 0.11	0.79 \pm 0.02	0.68 \pm 0.02	0.78 \pm 0.02	0.73 \pm 0.03
μ_{H_2}	0.79 \pm 0.01	0.79 \pm 0.03	0.84 \pm 0.01	0.56 \pm 0.14	0.81 \pm 0.03	0.81 \pm 0.01	0.84 \pm 0.03	0.81 \pm 0.03
μ_{CH_4}	0.74 \pm 0.06	0.67 \pm 0.05	0.82 \pm 0.01	0.63 \pm 0.07	0.70 \pm 0.05	0.76 \pm 0.01	0.82 \pm 0.02	0.78 \pm 0.05
μ_{He}	0.76 \pm 0.01	0.76 \pm 0.04	0.80 \pm 0.02	0.46 \pm 0.17	0.77 \pm 0.04	0.78 \pm 0.03	0.80 \pm 0.03	0.77 \pm 0.04
μ_{N_2}	0.66 \pm 0.07	0.71 \pm 0.02	0.77 \pm 0.01	0.20 \pm 0.09	0.74 \pm 0.01	0.74 \pm 0.02	0.75 \pm 0.03	0.61 \pm 0.05
μ_{O_2}	0.72 \pm 0.02	0.78 \pm 0.03	0.82 \pm 0.00	0.46 \pm 0.06	0.82 \pm 0.02	0.71 \pm 0.01	0.80 \pm 0.02	0.75 \pm 0.03

Table S2. Comparison of predictive performance (R^2 scores \pm standard deviation) for polymer properties across various machine learning models using the embeddings generated from Uni-Mol as input features.

Property	RandomForest	LinearRegression	SVR	DecisionTree	RidgeRegression	AdaBoost	GradientBoosting	XGBoost
ρ	0.62 \pm 0.01	0.62 \pm 0.03	0.66 \pm 0.01	0.19 \pm 0.17	0.67 \pm 0.03	0.57 \pm 0.02	0.72 \pm 0.03	0.67 \pm 0.03
T_g	0.80 \pm 0.00	0.81 \pm 0.01	0.66 \pm 0.00	0.57 \pm 0.02	0.82 \pm 0.01	0.74 \pm 0.01	0.82 \pm 0.00	0.82 \pm 0.01
T_m	0.60 \pm 0.01	0.26 \pm 0.03	0.28 \pm 0.00	0.17 \pm 0.03	0.35 \pm 0.02	0.57 \pm 0.01	0.65 \pm 0.00	0.63 \pm 0.01
T_d	0.56 \pm 0.01	0.46 \pm 0.02	0.38 \pm 0.00	0.14 \pm 0.04	0.47 \pm 0.02	0.49 \pm 0.01	0.59 \pm 0.01	0.59 \pm 0.01
σ_y	-0.22 \pm 0.87	-0.02 \pm 0.15	0.19 \pm 0.01	-3.83 \pm 6.32	-0.01 \pm 0.15	0.42 \pm 0.12	0.13 \pm 0.56	-1.45 \pm 3.53
σ_b	0.30 \pm 0.05	-0.09 \pm 0.11	0.20 \pm 0.01	-0.44 \pm 0.39	-0.08 \pm 0.11	0.34 \pm 0.05	0.32 \pm 0.11	0.29 \pm 0.18
ϵ_b	0.32 \pm 0.05	-0.45 \pm 0.09	0.22 \pm 0.01	-0.25 \pm 0.07	-0.41 \pm 0.08	0.32 \pm 0.03	0.40 \pm 0.01	0.31 \pm 0.04
E	0.30 \pm 0.08	-0.04 \pm 0.03	0.12 \pm 0.01	-0.06 \pm 0.26	-0.02 \pm 0.02	0.29 \pm 0.06	0.39 \pm 0.04	0.28 \pm 0.07
σ	0.32 \pm 0.04	0.06 \pm 0.12	0.02 \pm 0.00	-0.15 \pm 0.10	0.07 \pm 0.11	0.35 \pm 0.05	0.39 \pm 0.04	0.33 \pm 0.04
E_{gc}	0.77 \pm 0.01	0.64 \pm 0.01	0.86 \pm 0.00	0.54 \pm 0.05	0.68 \pm 0.01	0.75 \pm 0.00	0.82 \pm 0.00	0.80 \pm 0.02
X_c	0.27 \pm 0.02	0.07 \pm 0.07	-0.01 \pm 0.01	-0.47 \pm 0.34	0.08 \pm 0.07	0.30 \pm 0.05	0.31 \pm 0.03	0.26 \pm 0.08
E_{gb}	0.84 \pm 0.03	0.90 \pm 0.01	0.89 \pm 0.01	0.65 \pm 0.06	0.90 \pm 0.01	0.87 \pm 0.01	0.89 \pm 0.01	0.85 \pm 0.03
E_{at}	0.75 \pm 0.03	0.94 \pm 0.01	0.81 \pm 0.03	0.62 \pm 0.06	0.94 \pm 0.01	0.77 \pm 0.03	0.85 \pm 0.02	0.80 \pm 0.02
E_{ca}	0.70 \pm 0.03	0.91 \pm 0.01	0.83 \pm 0.02	0.49 \pm 0.12	0.91 \pm 0.01	0.79 \pm 0.02	0.84 \pm 0.02	0.75 \pm 0.03
E_i	0.68 \pm 0.02	0.74 \pm 0.02	0.80 \pm 0.01	0.30 \pm 0.11	0.74 \pm 0.02	0.70 \pm 0.03	0.72 \pm 0.04	0.62 \pm 0.04
n_c	0.71 \pm 0.03	0.72 \pm 0.05	0.69 \pm 0.03	0.52 \pm 0.10	0.72 \pm 0.05	0.72 \pm 0.04	0.74 \pm 0.02	0.69 \pm 0.04
μ_{CO_2}	0.61 \pm 0.02	0.65 \pm 0.05	0.79 \pm 0.01	0.28 \pm 0.18	0.66 \pm 0.05	0.64 \pm 0.02	0.69 \pm 0.02	0.64 \pm 0.05
μ_{H_2}	0.65 \pm 0.05	0.77 \pm 0.03	0.79 \pm 0.01	0.41 \pm 0.09	0.78 \pm 0.03	0.69 \pm 0.03	0.73 \pm 0.03	0.66 \pm 0.05
μ_{CH_4}	0.66 \pm 0.04	0.73 \pm 0.07	0.79 \pm 0.01	0.36 \pm 0.17	0.74 \pm 0.07	0.76 \pm 0.02	0.77 \pm 0.01	0.72 \pm 0.05
μ_{He}	0.66 \pm 0.02	0.74 \pm 0.04	0.75 \pm 0.02	0.43 \pm 0.10	0.78 \pm 0.02	0.65 \pm 0.03	0.70 \pm 0.02	0.65 \pm 0.07
μ_{N_2}	0.64 \pm 0.02	0.68 \pm 0.02	0.75 \pm 0.00	0.34 \pm 0.10	0.69 \pm 0.02	0.69 \pm 0.01	0.69 \pm 0.03	0.67 \pm 0.02
μ_{O_2}	0.68 \pm 0.03	0.70 \pm 0.04	0.78 \pm 0.01	0.42 \pm 0.08	0.71 \pm 0.03	0.68 \pm 0.02	0.74 \pm 0.02	0.66 \pm 0.04

Table S3. Comparison of predictive performance (R^2 scores \pm standard deviation) for polymer properties across various machine learning models using Morgan Fingerprint as input features.

Property	RandomForest	LinearRegression	SVR	DecisionTree	RidgeRegression	AdaBoost	GradientBoosting	XGBoost	MLP
ρ	0.57 \pm 0.04	-2.51 \pm 1.10	0.41 \pm 0.01	0.42 \pm 0.08	-0.49 \pm 0.25	0.39 \pm 0.04	0.54 \pm 0.01	0.62 \pm 0.02	0.38 \pm 0.04
T_g	0.86 \pm 0.00	0.79 \pm 0.01	0.35 \pm 0.00	0.75 \pm 0.00	0.79 \pm 0.01	0.68 \pm 0.01	0.81 \pm 0.00	0.87 \pm 0.00	0.85 \pm 0.00
T_m	0.73 \pm 0.01	0.22 \pm 0.09	0.11 \pm 0.00	0.54 \pm 0.03	0.24 \pm 0.08	0.50 \pm 0.02	0.67 \pm 0.01	0.76 \pm 0.01	0.71 \pm 0.01
T_d	0.68 \pm 0.02	0.54 \pm 0.01	0.19 \pm 0.00	0.47 \pm 0.02	0.54 \pm 0.01	0.46 \pm 0.02	0.60 \pm 0.00	0.72 \pm 0.01	0.64 \pm 0.02
σ_y	0.41 \pm 0.53	-0.82 \pm 0.60	0.52 \pm 0.02	0.58 \pm 0.13	0.22 \pm 0.24	0.42 \pm 0.05	0.72 \pm 0.06	0.62 \pm 0.17	0.27 \pm 0.10
σ_b	0.27 \pm 0.12	-1.07 \pm 0.78	0.32 \pm 0.02	-0.43 \pm 0.04	0.43 \pm 0.12	-0.24 \pm 0.20	0.37 \pm 0.10	0.28 \pm 0.13	0.21 \pm 0.05
ϵ_b	0.33 \pm 0.03	-4.21 \pm 2.33	0.45 \pm 0.01	0.00 \pm 0.04	0.19 \pm 0.04	0.26 \pm 0.04	0.40 \pm 0.03	0.34 \pm 0.04	0.29 \pm 0.04
E	0.64 \pm 0.04	-1.00 \pm 0.89	0.40 \pm 0.02	0.32 \pm 0.19	0.55 \pm 0.07	0.16 \pm 0.28	0.53 \pm 0.06	0.46 \pm 0.03	0.37 \pm 0.05
σ	0.38 \pm 0.04	-0.22 \pm 0.25	0.18 \pm 0.00	-0.01 \pm 0.04	0.29 \pm 0.10	0.20 \pm 0.01	0.39 \pm 0.04	0.43 \pm 0.04	0.60 \pm 0.01
E_{gc}	0.85 \pm 0.01	0.67 \pm 0.02	0.78 \pm 0.00	0.74 \pm 0.02	0.67 \pm 0.02	0.69 \pm 0.01	0.82 \pm 0.01	0.86 \pm 0.01	0.82 \pm 0.01
X_c	0.39 \pm 0.06	-0.12 \pm 0.25	-0.04 \pm 0.01	-0.02 \pm 0.12	-0.03 \pm 0.20	0.30 \pm 0.02	0.34 \pm 0.05	0.28 \pm 0.08	0.42 \pm 0.04
E_{gb}	0.85 \pm 0.02	0.66 \pm 0.03	0.55 \pm 0.01	0.72 \pm 0.06	0.68 \pm 0.03	0.79 \pm 0.02	0.86 \pm 0.01	0.85 \pm 0.01	0.76 \pm 0.03
E_{at}	0.75 \pm 0.03	0.72 \pm 0.04	0.32 \pm 0.03	0.65 \pm 0.03	0.71 \pm 0.05	0.73 \pm 0.02	0.82 \pm 0.02	0.81 \pm 0.03	-4.57 \pm 1.33
E_{ca}	0.82 \pm 0.02	0.61 \pm 0.03	0.40 \pm 0.02	0.75 \pm 0.05	0.62 \pm 0.04	0.76 \pm 0.02	0.83 \pm 0.02	0.83 \pm 0.02	0.79 \pm 0.01
E_i	0.73 \pm 0.02	0.57 \pm 0.06	0.52 \pm 0.02	0.56 \pm 0.09	0.62 \pm 0.06	0.67 \pm 0.02	0.77 \pm 0.01	0.76 \pm 0.03	-0.01 \pm 0.04
n_c	0.65 \pm 0.05	0.21 \pm 0.07	0.46 \pm 0.02	0.42 \pm 0.11	0.47 \pm 0.10	0.66 \pm 0.03	0.70 \pm 0.03	0.69 \pm 0.06	0.36 \pm 0.17
μ_{CO_2}	0.74 \pm 0.02	0.35 \pm 0.17	0.61 \pm 0.01	0.49 \pm 0.12	0.52 \pm 0.05	0.65 \pm 0.01	0.76 \pm 0.01	0.73 \pm 0.04	0.29 \pm 0.07
μ_{H_2}	0.86 \pm 0.01	0.65 \pm 0.07	0.64 \pm 0.02	0.72 \pm 0.06	0.68 \pm 0.05	0.77 \pm 0.02	0.82 \pm 0.02	0.85 \pm 0.04	0.18 \pm 0.09
μ_{CH_4}	0.79 \pm 0.01	0.48 \pm 0.09	0.56 \pm 0.01	0.73 \pm 0.04	0.58 \pm 0.08	0.71 \pm 0.01	0.81 \pm 0.02	0.81 \pm 0.03	0.52 \pm 0.02
μ_{He}	0.79 \pm 0.01	0.42 \pm 0.13	0.60 \pm 0.02	0.67 \pm 0.05	0.57 \pm 0.06	0.77 \pm 0.02	0.80 \pm 0.01	0.77 \pm 0.01	-0.47 \pm 0.19
μ_{N_2}	0.74 \pm 0.01	0.35 \pm 0.10	0.61 \pm 0.01	0.63 \pm 0.06	0.54 \pm 0.03	0.66 \pm 0.01	0.76 \pm 0.01	0.78 \pm 0.02	0.12 \pm 0.09
μ_{O_2}	0.71 \pm 0.03	0.44 \pm 0.09	0.64 \pm 0.01	0.56 \pm 0.03	0.61 \pm 0.04	0.65 \pm 0.01	0.75 \pm 0.02	0.78 \pm 0.04	0.43 \pm 0.02

Table S4. Comparison of predictive performance (R^2 scores \pm standard deviation) for polymer properties across various machine learning models using the molecular descriptors as input features.

Property	RandomForest	SVR	DecisionTree	AdaBoost	GradientBoosting	XGBoost	MLP
ρ	0.66 \pm 0.03	0.02 \pm 0.01	0.61 \pm 0.07	0.54 \pm 0.02	0.72 \pm 0.02	0.73 \pm 0.05	-0.06 \pm 0.08
T_g	0.85 \pm 0.00	0.02 \pm 0.00	0.71 \pm 0.02	0.74 \pm 0.00	0.83 \pm 0.00	0.87 \pm 0.00	0.87 \pm 0.00
T_m	0.64 \pm 0.01	0.01 \pm 0.00	0.42 \pm 0.06	0.53 \pm 0.01	0.66 \pm 0.01	0.68 \pm 0.02	0.69 \pm 0.03
T_d	0.69 \pm 0.01	0.02 \pm 0.00	0.41 \pm 0.06	0.48 \pm 0.01	0.63 \pm 0.01	0.71 \pm 0.01	0.64 \pm 0.00
σ_y	0.47 \pm 0.26	-0.03 \pm 0.01	0.32 \pm 0.34	0.56 \pm 0.30	0.35 \pm 0.34	0.12 \pm 0.39	0.19 \pm 0.11
σ_b	0.45 \pm 0.12	-0.07 \pm 0.00	-0.03 \pm 0.44	0.37 \pm 0.16	0.45 \pm 0.13	0.48 \pm 0.02	0.27 \pm 0.08
ϵ_b	0.17 \pm 0.03	-0.06 \pm 0.00	-0.28 \pm 0.15	0.12 \pm 0.04	0.14 \pm 0.05	0.29 \pm 0.13	-0.04 \pm 0.06
E	0.40 \pm 0.12	-0.07 \pm 0.01	-0.39 \pm 0.31	0.14 \pm 0.13	0.35 \pm 0.10	0.10 \pm 0.08	0.38 \pm 0.05
σ	0.47 \pm 0.05	-0.17 \pm 0.01	0.15 \pm 0.10	0.36 \pm 0.04	0.44 \pm 0.02	0.39 \pm 0.10	0.34 \pm 0.10
E_{gc}	0.86 \pm 0.01	0.00 \pm 0.00	0.75 \pm 0.02	0.74 \pm 0.01	0.85 \pm 0.00	0.88 \pm 0.01	0.83 \pm 0.01
X_c	0.39 \pm 0.02	-0.08 \pm 0.02	-0.00 \pm 0.13	0.36 \pm 0.02	0.39 \pm 0.04	0.31 \pm 0.05	0.49 \pm 0.02
E_{gb}	0.90 \pm 0.01	-0.06 \pm 0.01	0.84 \pm 0.01	0.88 \pm 0.01	0.91 \pm 0.01	0.91 \pm 0.01	0.84 \pm 0.04
E_{at}	0.88 \pm 0.04	-0.00 \pm 0.00	0.79 \pm 0.08	0.86 \pm 0.02	0.92 \pm 0.03	0.90 \pm 0.02	-4.16 \pm 0.81
E_{ea}	0.80 \pm 0.01	-0.09 \pm 0.04	0.68 \pm 0.03	0.80 \pm 0.01	0.84 \pm 0.01	0.79 \pm 0.02	-25.96 \pm 33.81
E_i	0.73 \pm 0.02	-0.10 \pm 0.04	0.42 \pm 0.03	0.68 \pm 0.02	0.72 \pm 0.03	0.69 \pm 0.05	-52.32 \pm 23.35
n_c	0.78 \pm 0.04	-0.07 \pm 0.02	0.58 \pm 0.05	0.80 \pm 0.03	0.83 \pm 0.05	0.82 \pm 0.03	-0.25 \pm 0.26
μ_{CO_2}	0.75 \pm 0.03	-0.06 \pm 0.00	0.51 \pm 0.09	0.64 \pm 0.01	0.75 \pm 0.02	0.74 \pm 0.03	0.14 \pm 0.18
μ_{H_2}	0.76 \pm 0.03	-0.03 \pm 0.01	0.61 \pm 0.09	0.73 \pm 0.01	0.79 \pm 0.02	0.79 \pm 0.03	0.28 \pm 0.07
μ_{CH_4}	0.79 \pm 0.01	-0.03 \pm 0.01	0.72 \pm 0.01	0.74 \pm 0.02	0.79 \pm 0.01	0.80 \pm 0.01	0.29 \pm 0.15
μ_{He}	0.70 \pm 0.06	-0.08 \pm 0.02	0.49 \pm 0.14	0.66 \pm 0.05	0.69 \pm 0.07	0.65 \pm 0.05	-0.02 \pm 0.38
μ_{N_2}	0.71 \pm 0.01	-0.04 \pm 0.01	0.48 \pm 0.08	0.65 \pm 0.01	0.73 \pm 0.03	0.70 \pm 0.03	0.32 \pm 0.13
μ_{O_2}	0.69 \pm 0.04	-0.03 \pm 0.01	0.44 \pm 0.09	0.64 \pm 0.03	0.71 \pm 0.03	0.69 \pm 0.04	0.61 \pm 0.06

Table S5. Comparison of predictive performance (mean R^2 scores \pm standard deviation) across various polymer properties for different models. The data for polyBERT,¹¹ Transpolymer,²⁹ and single task (ST) polyGNN²⁸ were obtained from their original paper.

Property	PolyLLMem	PolymerBERT	Transpolymer	ST polyGNN
Train data	0.02M	100M	5M	-
ρ	0.83 ± 0.01	0.75 ± 0.03	-	0.90 ± 0.01
T_g	0.89 ± 0.01	0.92 ± 0.01	-	0.89 ± 0.01
T_m	0.77 ± 0.01	0.84 ± 0.02	-	0.76 ± 0.03
T_d	0.73 ± 0.01	0.70 ± 0.03	-	0.66 ± 0.02
σ_y	0.56 ± 0.12	0.80 ± 0.08	-	-
σ_b	0.32 ± 0.07	0.76 ± 0.05	-	0.50 ± 0.20
ϵ_b	0.24 ± 0.04	0.60 ± 0.06	-	-
E	0.52 ± 0.06	0.75 ± 0.70	-	0.43 ± 0.20
σ	0.45 ± 0.05	-	-	-
E_{gc}	0.92 ± 0.01	0.89 ± 0.02	0.92	0.92 ± 0.01
X_c	0.40 ± 0.03	0.45 ± 0.11	0.50	0.40 ± 0.07
E_{gb}	0.94 ± 0.01	0.93 ± 0.01	0.93	0.84 ± 0.07
E_{at}	0.96 ± 0.01	0.85 ± 0.02	-	0.96 ± 0.10
E_{ea}	0.92 ± 0.01	0.93 ± 0.03	0.91	0.78 ± 0.10
E_i	0.81 ± 0.03	0.82 ± 0.07	0.84	-
n_c	0.83 ± 0.01	0.86 ± 0.06	0.82	0.54 ± 0.30
μ_{CO_2}	0.83 ± 0.02	0.94 ± 0.02	-	0.87 ± 0.03
μ_{H_2}	0.85 ± 0.03	0.97 ± 0.01	-	0.91 ± 0.02
μ_{CH_4}	0.87 ± 0.03	0.95 ± 0.03	-	0.90 ± 0.03
μ_{He}	0.81 ± 0.02	0.95 ± 0.02	-	0.88 ± 0.04
μ_{N_2}	0.79 ± 0.01	0.97 ± 0.01	-	0.83 ± 0.10
μ_{O_2}	0.87 ± 0.01	0.96 ± 0.01	-	0.85 ± 0.03

Table S6. Finetuning hyperparameters for PolyLLMem.

Hyperparameter	Range
Batch size	{8, 64}
Hidden size	{512, 4096}
Rank	{4, 32}
Alpha	{4, 128}
Learning Rate	$\{5 \times 10^{-5}, 1 \times 10^{-4}\}$
Weight Decay	{0.001, 0.00001}
Dropout rate	{0.0, 0.5}